Original Article

OSL chronology of a Palaeolithic site in a humid subtropical mountainous area of southeast China

JIN Jian-hui[1,2]* (iD) https://orcid.org/0000-0002-1924-4609; ✉ e-mail: geojjh@fjnu.edu.cn

WANG Xiao-yang[3] (iD) https://orcid.org/0000-0002-1701-2580; e-mail: 472230589@qq.com

ZHOU Zhen-yu[4] (iD) https://orcid.org/0000-0002-8719-3604; e-mail: zzy529@msn.com

HUANG Yun-ming[3,5] (iD) https://orcid.org/0000-0001-7133-3986; e-mail: 286413079@qq.com

FAN Xue-chun[3,6] (iD) https://orcid.org/0000-0003-0367-242X; e-mail: xchunfan@126.com

ZUO Xin-xin[1,2] (iD) https://orcid.org/0000-0002-1693-0275; e-mail: zuoxinxin@fjnu.edu.cn

LI Zhi-zhong[1] (iD) https://orcid.org/0000-0003-0035-9892; e-mail: lizz@fjnu.edu.cn

LING Zhi-yong[7] (iD) https://orcid.org/0000-0002-3322-0830; e-mail: 1572501160@qq.com

REN Yong-qing[1] (iD) https://orcid.org/0000-0002-6737-7246; e-mail: renyqing@163.com

LI Shu-tong[1] (iD) https://orcid.org/0000-0002-8030-4615; e-mail: 103371953@qq.com

*Corresponding author

1 School of Geographical Sciences, Fujian Normal University, Fuzhou 350007, China

2 Center for Southeast environmental archaeology, Fujian Normal University, Fuzhou 350007, China

3 Fujian Institute of Archaeology, Fuzhou 350001, China

4 The institute of Archaeology, Chinese Academy of Social Sciences, Beijing 100710, China

5 School of Humanities, Minjiang University, Minhou 350108, China

6 Pingtan International Institute of Austronesian Archaeology, Pingtan 350400, China

7 Qinghai Institute of Salt Lakes, Chinese Academy of Sciences, Xi'ning 810008, China

Abstract: The timing of Palaeolithic human activities in South China is still controversial because of the lack of a reliable chronology of archaeological sites. The Longdengshan Palaeolithic site (LPS), located close to the Wuyi Mountain of South China, represents the first discovered and scientifically excavated Middle Palaeolithic site in the Fujian Province. This site is of considerable significance for studying the diffusion and cultural connotation of early Homo sapiens in southern China. In this study, we present optically stimulated luminescence (OSL) ages obtained from medium-grained quartz collected at the LPS. The single-aliquot regenerative-dose measurements of red soil deposits collected at the same site yielded internally and stratigraphically consistent ages and similar errors, indicating a potential ability of the technique, and also reflecting

the influence of various sedimentary facies on the test results. Our results indicate that the 38-63 μm quartz grains were generally partially-bleached and had large values of over-dispersion in the palaeo-reticulated laterites of west Fujian. Some samples yielded unsatisfactory results, suggesting that the degree of bleaching of diluvial and alluvial deposits should be properly assessed before dating. We did not detect any enrichment/depletion of U, Th and radioactive disequilibrium. The effect of chemical weathering on the dose rate estimation was negligible. Therefore, we used a central age model and the maximum age model to calculate the age of two samples, respectively, and the minimum age model to calculate the ages of the rest of the samples. The OSL ages of the samples ranged from 27.09 ± 2.30 ka to 54.65 ± 7.39 ka for the 38-63 μm quartz size fraction, and roughly corresponded to the Marine Isotope Stage 3. In addition, three ages out of five are based on the calculation of minimum ages in this research, which needs to be further verified by other dating methods.

1 Introduction

At the beginning of the 20th century, scholars from several countries began to uncover Palaeolithic remains in South China; some of these discoveries, despite having being reported (Pei 1955), lack solid chronological evidence (Li 1982). Remains of the Palaeolithic culture were discovered in South China only in the 1950s. The discovery of more sites and their study has helped us gain a comprehensive understanding of this culture (Jia and Qiu 1960; Olsen and Miller-Antonio 1992; Zhang 1983). However, many scientific problems (e.g. site chronology) still need to be solved (Wang 1997).

The soil in South China is generally acidic and organic matter is difficult to preserve. Thus, few palaeontological fossils have been found in the soil. As a result, it is impossible to determine any age by palaeontological or ¹⁴C dating methods. In recent years, several Palaeolithic sites have been found and excavated in Fujian (Southeast China), which is an area of considerable significance for studying the diffusion and cultural connotation of early Homo sapiens in southern China. However, most of the sites in this area have not been well dated due to the lack of suitable materials.

The optically stimulated luminescence (OSL) technique exceeds the dating range limits of the radiocarbon method, and has already become a widely used and successful tool for estimating the ages of different types of sediments in the Palaeolithic sites of northern China (Guo et al. 2017; Li et al. 2017; Nian et al. 2015). Recent studies have shown that OSL can be employed to date Palaeolithic sites in southwest China (under a subtropical monsoon climate) (Hu et al. 2019; Zhang et al. 2019), but the effect of weathering on the dose rate estimation should be investigated on a case-by-case basis (Zhang et al. 2019). The aim of this study is to provide more reliable age estimates of the human occupation and its 'latest' granite tools industry at Longdengshan Palaeolithic site (LPS) by applying OSL dating to quartz grains. Based on the OSL signals (obtained from quartz using the single-aliquot regenerative-dose (SAR) protocol), we determined the age of the LPS in western Fujian Province, China (Fan et al. 2019), in addition, we discussed the relationship between human activities and their association with climate change.

2 Study Area

The Jiangle County extends at the southeast foot of the Wuyi Mountain. The mountain is oriented in a northeast – southwest direction, similarly to the Jin River (i.e. the largest tributary of the Futun River, which divides the county into roughly equal southern and northern parts. The Longdengshan Palaeolithic Site (LPS) (26°42'47" N, 117°28'17" E), discovered in August 2018, is located to the southeast of Dutou Village (Jiangle County, Fujian Province). More precisely, it is positioned on a low hill (the Longdeng Mount) to the west of the Xinxing plasma station in the Jiangle County, 800 meters to the west of the Jin River (Fig. 1). The LPS is the firstly discovered and scientifically excavated open-air site of the Middle Palaeolithic period in the Fujian Province. The discovery of this site expanded the distribution range of Paleolithic cultural relics in Fujian Province, and provided materials for the comparison of Paleolithic cultural properties in different regions in Fujian Province.

At the bottom of the site stratum is a granite weathering crust covered with reticulated laterite and thin layers of homogeneous laterite. The grain size
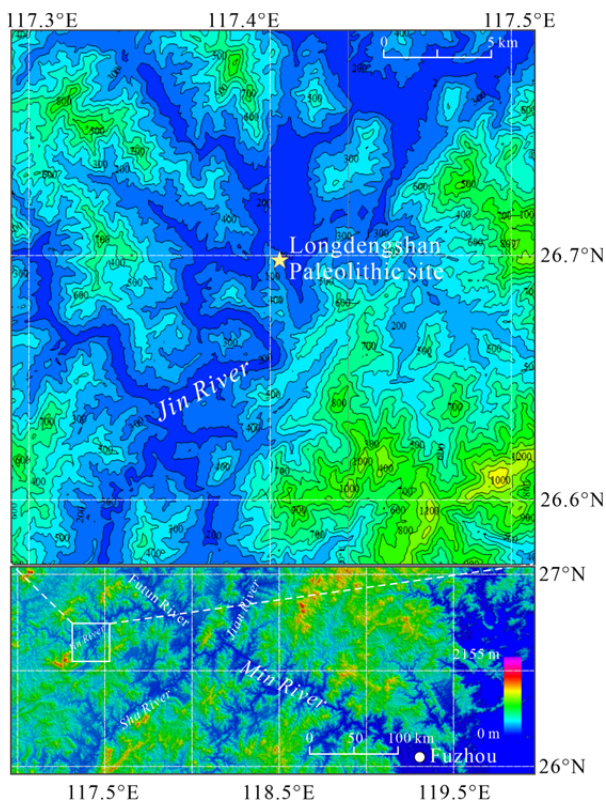
Fig. 1 Geomorphic features of the study area and the location of the Longdengshan Palaeolithic site.

parameters show that the reticulated laterite in Jiangle area is similar to the reticulated laterite in other areas of Fujian Province, but completely different from the reticulated laterite of Xuancheng, which also indicates that the reticulated laterite in Jiangle area does not belong to aeolian sediment. From the perspective of geomorphic features, these reticulated laterites are distributed equally on river terraces and are generally interbedded with gravel beds in sedimentary strata. Such sedimentary characteristics are common not only in the reticulated laterites in Fujian Province, but also in the reticulated laterites of Jiangxi and Guangdong Provinces. The SEM results show that the surface of quartz particles in reticulated laterite is smooth, and there are dissolution cracks, and there are a lot of directional pits left by mechanical impact on the surface, which indicates that the quartz particles have experienced a strong hydrodynamic process. The reticulated laterite in Jiangle should be the product of strong chemical weathering after alluvial and diluvial deposition.

In order to further understand the chronology, burial situation and cultural connotation of the site, a trial excavation was conducted jointly on-site by the Institute of Archaeology, Chinese Academy of Social

Sciences and the Institute of Archaeology, Fujian Provincial Museum in October 2018. The exploration quadrant was extended in the southeast-northwest direction, and the actual excavation area of the quadrat is 18 m². The stratigraphy of the excavation site can be summarized as follows:

The 7th layer, composed of granite bedrock (Fig. 2).

The 6th layer (thickness ~25-53 cm) represented by reticulated laterite. The surface of this laterite contains a relatively high amount of gravel and a small amount of chipped stone tools.

The 5th layer (thickness ~21-55 cm), represented by hard reticulated laterite with intermittent gravel bands on the surface and containing a small amount of chipped stone tools.

The 4th layer (thickness ~105 cm), represented by reticulated laterite and distributed only in the southeastern part of the excavation site. Two chipped stone tools were excavated from this layer.

The 3rd layer (thickness ~10-30 cm), represented by hard reticulated laterite, containing a small amount of gravel. Two chipped stone tools were found in there.

The 2nd layer (thickness ~20-35 cm), composed of red clay, hard soil, and a small amount of gravel, but no cultural relics.

The 1st layer, representing a modern disturbance layer (thickness 10-15 cm), and mainly composed of construction waste, including a large number of stones and cement blocks.

3　Methods

3.1 Sample collection

Over the last 30 years, OSL dating has become one of the most widely used numerical methods to determine burial ages in late Quaternary sediments located in a variety of depositional environments (Aitken 1998; Fu and Li 2013; Gao et al. 2017; Jacobs et al. 2011; Lai et al. 2013; Li and Li 2011; Nian et al. 2018; Zhang et al. 2015; Zhang et al. 2008). Five OSL samples (2019051 - 2019055) were collected for OSL dating from the LPS site by using metal tubes (Fig. 2). The burial time of quartz or feldspar grains could be estimated from the intensity of the OSL signal, by converting it into an equivalent dose (D_e) and by dividing the D_e by the environmental dose rate (Aitken 1998; Murray and Wintle 2000). The latter represents the rate of ionizing radiation supply to the
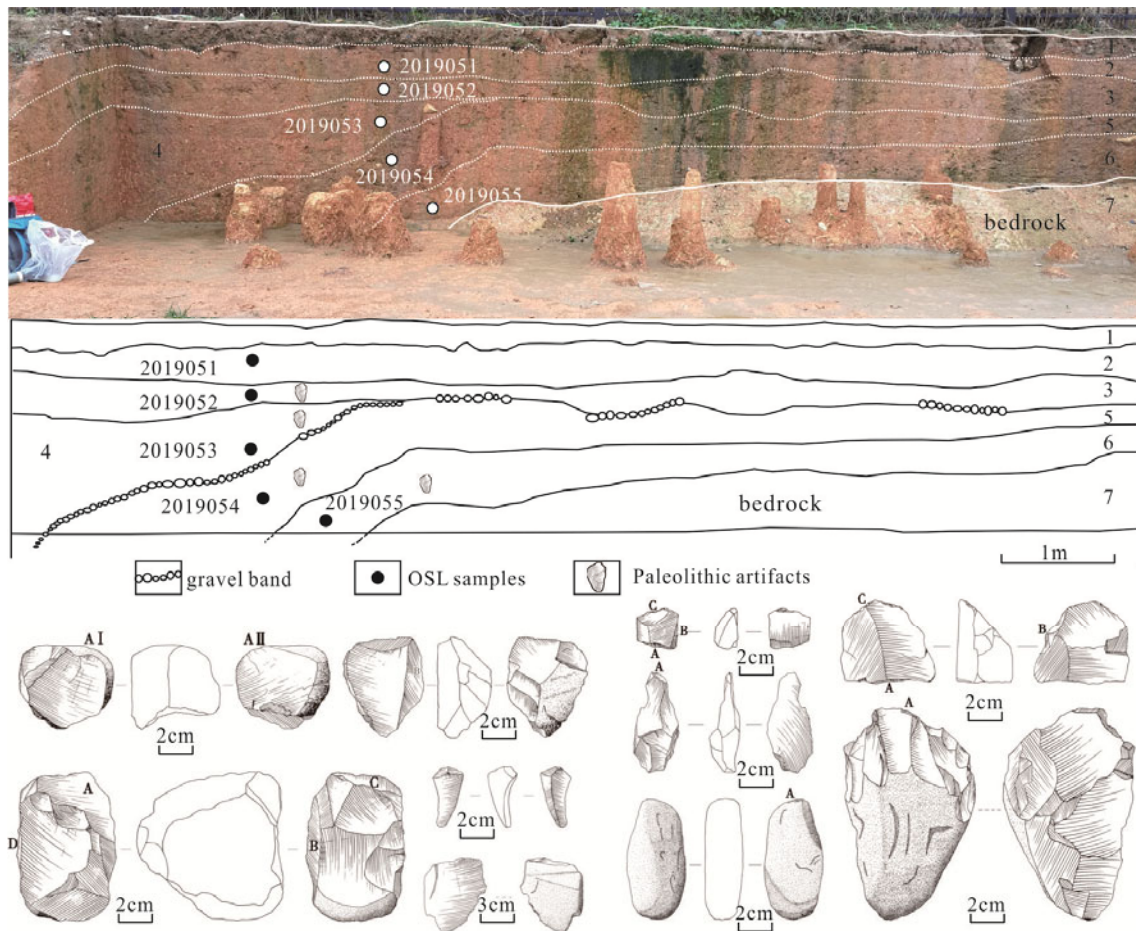
Fig. 2 Photograph and line drawing showing the stratigraphic divisions. The approximate locations and the line drawings of the stone tools recovered from the excavation unit. The OSL sampling locations in the LPS (South China) are also shown.

grain over the burial period from environmental sources of alpha, beta and gamma radiations (deriving from the decay of radionuclides in the U and Th decay chains and of ^{40}K), as well as from cosmic rays (Adamiec and Aitken 1998; Aitken 1998).

3.2 Sample preparation and equivalent dose determination

The grain size of reticulated laterite in the LPS section is mainly composed of silt, followed by clay and sand, so we chose fraction of 38-63 μm as the test object. The preparation and measurement of the OSL samples were performed under dim red light in order to avoid optical bleaching. After removing the outer layers of the samples, 30% hydrogen peroxide (H_2O_2) and 10% hydrochloric acid (HCl) were applied to the inner cores, so to eliminate the organic matter and carbonate components, respectively. Afterwards, the raw sediment samples were rinsed and wet-sieved to

retain the 38-63 μm grain size fraction. Then they were etched by applying 40% hydrofluoric acid (HF) for 40 min, in order to isolate the quartz grains. The purity of the quartz separates was determined based on their OSL-IR (infrared) depletion ratios (>0.9) (Duller 2003) and thermoluminescence (TL) measurements (with a TL peak of 110 °C) (Li et al. 2002).

The OSL measurements were carried out at the luminescence dating laboratory of Fujian Normal University using an automated Risø TL/OSL DA-20C/D reader. Blue LED (k = 470 ± 20 nm) were used for the stimulation. The OSL signal was explored through a 7.5mm Hoya U-340 filter, and a $^{90}Sr/^{90}Y$ beta source was used for the laboratory irradiation (Bøtter-Jensen et al., 2003). The dose rate for a medium quartz grain from the beta source was 0.09 Gy/s.

The equivalent doses (D_e) were measured following the SAR protocol (Murray and Wintle 2000).

The aliquots were stimulated at 130°C for 40 s. A preheat temperatures of 240°C and a cutheat temperature of 200°C were applied for 10 s and 0 s, respectively, were used on the basis of preheat plateau tests (Fig. 3). A blue light stimulation was conducted at 290°C for 40 s at the end of each SAR cycle to remove the remaining signals (Table 1). The acceptance criteria (recycling ratio limit is 10%; maximum recuperation is 5% of nature; maximum test dose error is 10%; test dose signal is more than 3 sigma above background) are applied for D_e values selection. A dose recovery test was carried out on 6 aliquots of sample 2019051, for which the nature OSL signals was removed after sunlight exposition for 48 h, and a known laboratory dose of 88.4 Gy was recovered using the SAR protocol, the mean value of dose recovery ratio was 0.93 ± 0.05.

3.3 Dose rate determination and OSL age calculation

For the dose rate determination, an inductively coupled plasma mass spectrometer (ICP-MS) and a flame photometer were used to determine the uranium (U), thorium (Th) and potassium (K) contents of the samples. The long-term water contents were assumed to be 15±5% and were added to each value in the age calculations (Jin et al. 2018). An alpha efficiency factor (a-value) of 0.035 ± 0.003 was considered for the 38-63 μm quartz grains (Lai et al. 2008). The attenuation factors (Brennan et al. 1991; Guérin et al. 2012) were used to calculate the alpha and beta dose rates. Finally, the dose rates and the final ages were calculated using the Dose Rate and Age Calculator (Durcan et al. 2015) and package 'Luminescence' version 0.9.10 of R language (convert_Concentration2DoseRate) (Riedesel et al. 2020).

4 Results

4.1 Environmental dose rate

The contents of U, Th and K, as well as the calculated environmental dose rates for the LPS, are listed in Table 2. The five samples showed similar variations in the U, Th and K contents considering the analytical uncertainty. In all cases, the values did not increase with depth (Table 2). The environmental

dose rates for the five simples ranged from 3.08±0.11 to 4.39±0.17 Gy/ka and are similar to those obtained for samples collected in the Fengshuizui site (Hunan Province), located in the same humid subtropical zone as the LPS, ranging from 3.81±0.13 to 4.10±0.14 Gy/ka (Zhang et al. 2019).
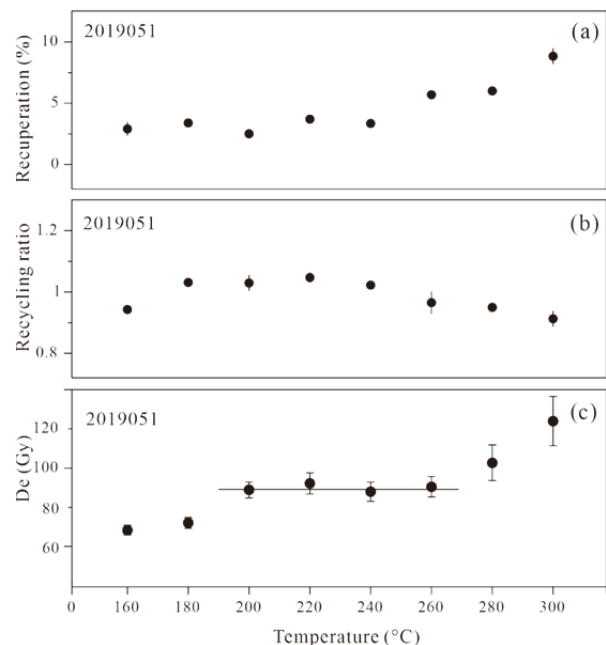
Fig. 3 Luminescence characteristics for quartz of sample 2019051 from the Longdengshan Palaeolithic site. (a) Recuperation values (from at least 3 aliquots at each temperature) for sample 2019051, (b) and (c) are their corresponding recycling ratios and preheat plateau results. The dashed lines represent the mean D_e values between 200 °C - 260 °C.

Table 1 Single-aliquot regenerative-dose (SAR) protocol used for age determination

Run	Treatment
1	Dose (except before first run)
2	Preheat (240°C for 10 s)
3	Optical stimulation with blue LEDs for 40 s at 130°C
4	Test dose
5	Cut heat at 200°C for 0 s
6	Optical stimulation with blue LEDs for 40 s at 130°C
7	Optical stimulation with blue LEDs for 40 s at 290°C
8	Return to 1

The environmental dose rate is one of the two main parameters affecting the OSL age, and can hence have a huge impact on its calculation (Jin et al. 2018; Smedley et al. 2020; Zhang et al. 2019; Zhang et al. 2008). Previous research has shown that

Table 2 Dosimetry of the samples from the Longdengshan Palaeolithic site

Sample No.		2019051	2019052	2019053	2019054	2019055
U (μg/g)		4.27±0.13	4.17±0.13	4.39±0.13	5.25±0.16	4.94±0.15
Th (μg/g)		19.7±0.59	22.7±0.68	24.6±0.74	31.3±0.94	31.1±0.93
U/Th		0.22	0.18	0.18	0.17	0.16
K (%)		0.91±0.03	1.08±0.03	1.17±0.04	1.44±0.04	1.29±0.04
Water content (%)		15±5	15±5	15±5	15±5	15±5
Depth (m)		0.3	0.6	1.0	1.3	1.5
Environmental dose rate (Gy/ka)	Beta	1.45±0.07	1.60±0.08	1.72±0.09	2.13±0.11	1.99±0.10
	Gamma	1.37±0.07	1.51±0.08	1.63±0.08	2.03±0.10	1.96±0.10
	Cosmic	0.19±0.02	0.18±0.02	0.17±0.02	0.16±0.02	0.15±0.02
	Total	3.08±0.11	3.37±0.12	3.58±0.13	4.39±0.17	4.18±0.16

chemical weathering can considerably influence the dose rate values in different humid subtropical regions of China (Jin et al. 2018; Zhang et al. 2008). In the process of weathering, U is more likely to migrate than Th: the higher the degree of weathering, the smaller the U/Th ratio (Zhang et al. 2008). From the top to bottom of the profile obtained for the LPS, the U/Th ratio did not show particular trends. The weathering degrees of the five samples, which were collected at different depth were similar; moreover, we did not detect any enrichment/depletion of U or Th. The U/Th ratios of samples 2019051 - 2019053 (0.18 - 0.22) were just slightly above those of samples 2019054 and 2019055 (0.16-0.17). The latter ratios were similar to those of modern coastal aeolian sand samples from Fujian (0.16 ± 0.01) (Jin et al. 2017). The similar U and Th contents and U/Th ratios obtained for the above five samples demonstrate that the sediments of the LPS section have very homogenous chemical compositions. The results obtained from the geochemical analysis of reticulated laterites adjacent to the study area (in Lushan, Jiangxi Province), showed that changes in other constant and rare earth elements were slight and consistent, except for Fe (Zhang et al. 2020). Additionally, a study conducted on a Palaeolithic site in the Hunan Province showed that easily weathered feldspar minerals and weathering products mainly composed of illite generally had similar contents of weathered sediments: sediments at different depths likely experienced similar degrees of weathering (Zhang et al. 2019). Therefore, we believe that the data in Table 2 can be used to calculate the environmental dose rates of the sediments contained in the cultural layers of the LPS. In addition, restricted by the arrangement of test time in relevant laboratories and field test conditions, the ages are based on a low number of aliquots measured (from 9 to 18) and no in situ

measurements were conducted for the gamma dose rate. These issues need to be further investigated in future studies.

4.2 Routine tests of the SAR protocol

To estimate the dependence of the D_e values on the preheat temperature, we conducted preheat plateau tests on the 38-63 μm quartz size fraction of sample 2019051 on natural aliquots: 10 s preheat at 160°C, 180°C, 200°C, 220°C, 240°C, 260°C, 280°C and 300°C were applied with a cut heat temperature of 160°C, following the SAR protocol.

In Fig. 3, a preheat plateau is observed between 200 and 260°C for the 38-63 μm quartz size fraction of sample 2019051; the corresponding recycling ratios and recuperation values are also shown. The recuperation values increase, especially in the case of high-temperature preheating (>260°C); still, they fell within 5%, except for the interval 260°C - 300°C (Fig. 3). The recycling ratios of this sample were within 10% of unity. Based on the results of the preheat plateau test, preheat and cut heat temperatures of 240°C and 200°C, respectively, were applied for the determination of the D_e values.

Fig. 4 shows the representative decay and dose response curves of the 38-63 μm quartz size fractions of samples 2019051 and 2019055. Their relative contributions to the bulk OSL signals demonstrates that the signals derived from the quartz grains were strong enough to be measured, while the rapid decay of the signals with the stimulation time indicates that they were dominated by the fast component (insets of Fig. 4). After subtracting a background integral of 32-40 s, the initial 0.8 s integral of the OSL decay curve was extracted and used to calculate the D_e ensuring that the signals were dominated by the fast component. The growth curves were fitted using
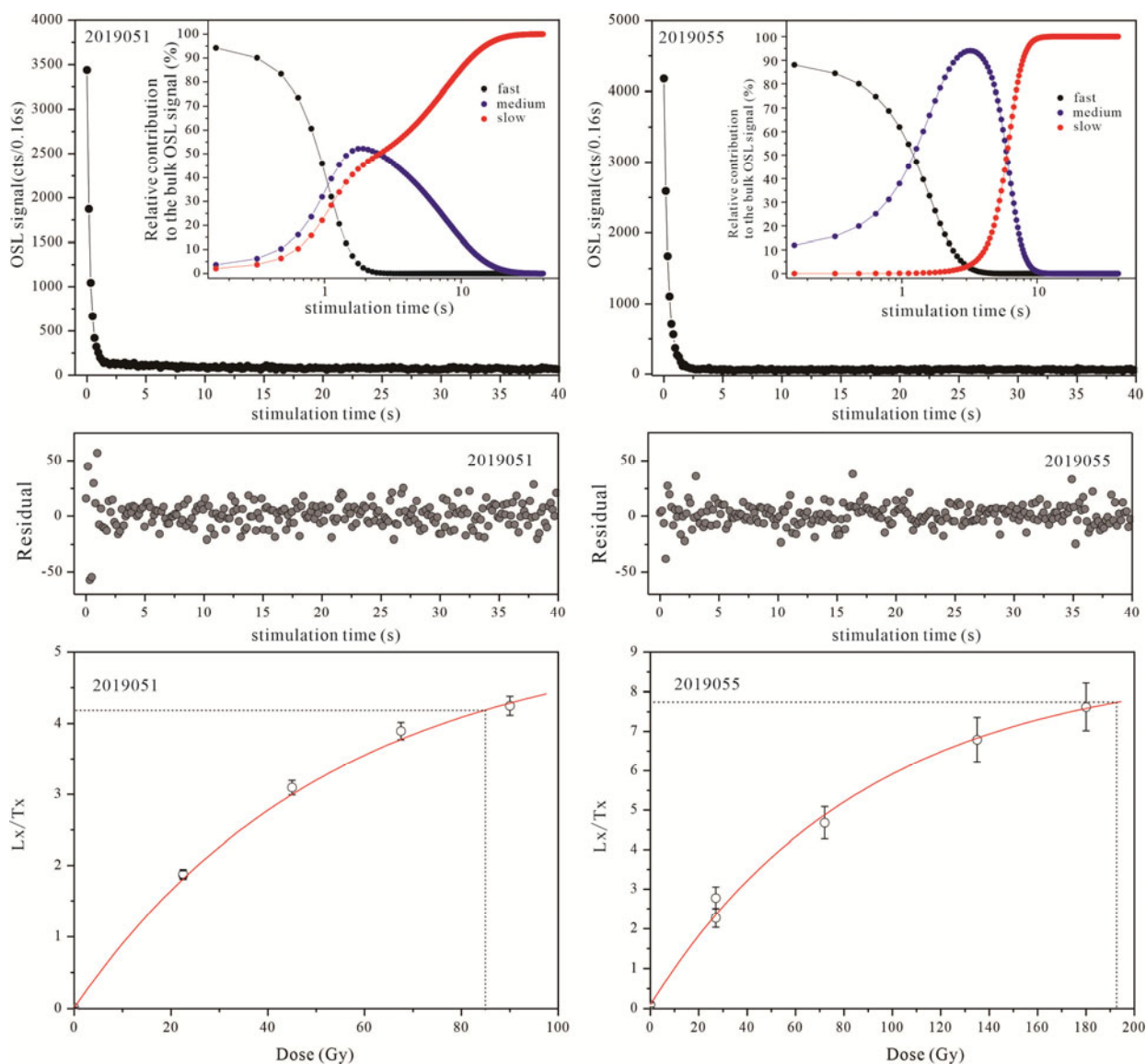
Fig. 4 Natural quartz OSL decay curves for samples 2019051 and 2019055, which were obtained from the analysis of the 38–63 μm quartz size fraction and the corresponding dose-response curves (constructed using the SAR protocol. Lx/Tx refers to ratio of lab signal and test signal). The insets show the relative contribution of the different signal components to the bulk OSL signal (%).

single saturating exponential functions (Fig. 4).

The laboratory doses were selected to approximate the equivalent palaeodoses. The dose recovery ratios (recovered/given dose) are within 10% of unity, which is receivable. The above results prove that the SAR protocol was appropriate for estimating the D_e values of the selected samples. This suggests a small variability between the aliquots of sample 2019051 comprised within the narrow regional trends and a local bedrock control on the intrinsic sources of scatter (Smedley et al. 2020).

4.3 OSL age estimates

Here, we use overdispersions (OD) 20% of the D_e distribution as the criteria for model selection. We calculated the D_e values of all the samples using the Maximum Age model (MaxAM) (Galbraith and Roberts 2012), central age model (CAM) and the Minimum Age model (MinAM) (Galbraith et al. 1999) (Table 2). The model ages, selected at the single-aliquot analytical scale, were based on the statistical procedure of Arnold et al. (2012) and are shown in bold in Table 3.

The distributions of the D_e values for samples 2019051-2019055 are presented as abanico plots and frequency density diagrams in Fig. 5. As shown in

Table 3 Summary of the quartz OSL ages obtained for the LPS

| Sample No.	2019051	2019052	2019053	2019054	2019055
Sedimentary horizon	2	3	4	5	6
CAM De values	117.88±23.32	165.19±14.51	233.39±20.45	63.34±17.60	194.24±12.54
MinAM De values	86.13±6.36	91.32±17.26	196.87±25.43	30.51±5.91	194.55±23.48
MaxAM De values	632.52±262.8	181.86±14.19	273.66±52.56	141.89±55.60	195.20±31.99
Numbers of aliquots	11/20	18/20	14/20	9/20	12/20
Over dispersion (%)	64.2±4.3	34.3±1.6	26.7±2.0	70.7±7.7	12.8±2.3
CAM ages	39.89±8.29	50.71±5.49	66.85±7.23	15.47±4.41	46.59±4.31
MinAM ages	27.93±2.30	27.09±5.22	54.65±7.39	6.95±1.37	46.58±5.89
MaxAM ages	210.5±88.48	55.11±5.52	77.71±15.71	32.90±13.06	47.56±8.38
Model selections	MinAM	MinAM	MinAM	MaxAM	CAM
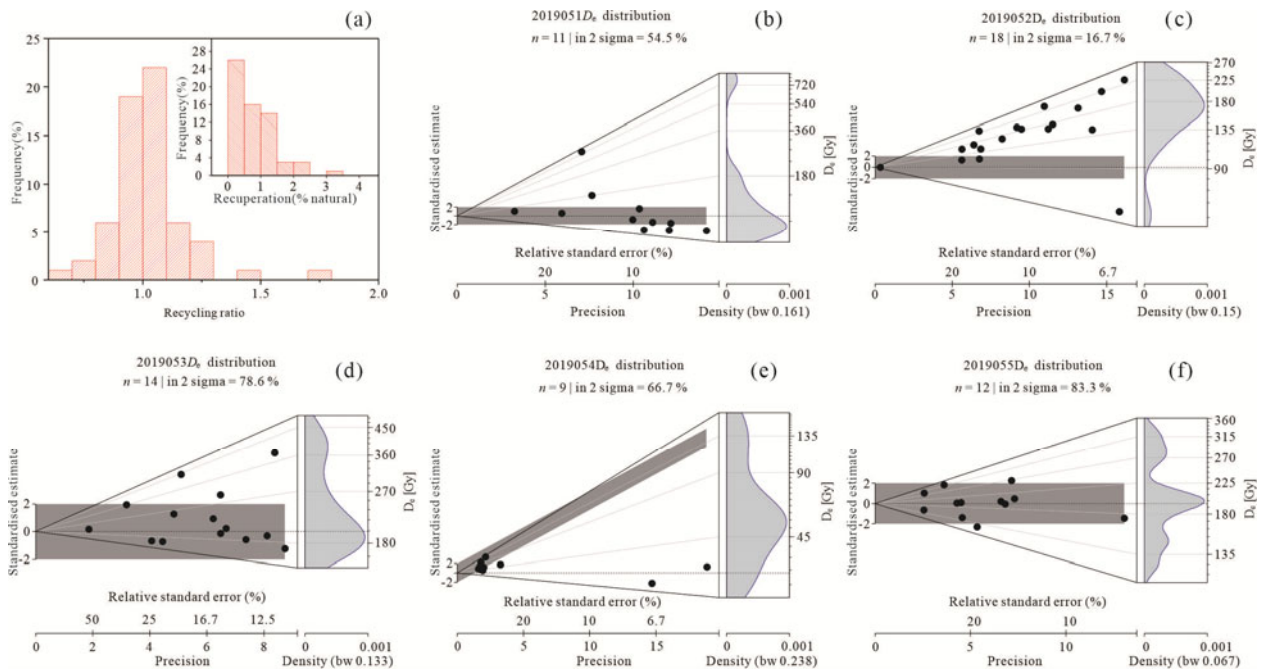
Fig. 5 (a) Histograms summarizing the recycling ratio and recuperation values. (b)-(f) Abanico plots and frequency density diagrams showing the distribution of the D_es values for all the OSL samples (the abanico plots were calculated and generated by package 'Luminescence' version 0.9.10 of R). The D_es values obtained by the MinAM for samples 2019051-2019053, the MaxAM for sample 2019054 and by the CAM for sample 2019055 are shaded (Galbraith and Roberts 2012; Galbraith et al. 1999).

Table 3, we calculated the D_e values for all the samples by CAM, MinAM and MaxAM model (Galbraith and Roberts 2012; Galbraith et al. 1999). The accuracy and precision of the OSL ages is highly dependent upon the application of the age models (Smedley et al. 2020). They did not yield identical D_e values for these samples because of high overdispersion values, except for sample 2019055. Four of these samples (e.g. 2019051-2019054) have overdispersions (OD) values >20%, while two of them (e.g. 2019051 and 2019054) have OD values >60% (64.2% and 70.7%, respectively). For sample 2019055, the OD value was <20% (12.8%); according to Arnold et al. (2012), this is a commonly accepted value for

well-bleached sedimentary quartz samples. Therefore, we used the central age model to calculate the age of sample 2019055, the MaxAM to calculate the ages of sample 2019054 which could be due to a mixing of fully bleached grains at the time of deposition with younger grains from intrusion and the MinAM to calculate the ages of samples 2019051-2019053 which might contain grains that were not completely bleached at the time of deposition. The age results range from 27.09 ± 2.30 ka to 54.65 ± 7.39 ka for the 38-63 μm quartz size fraction, indicating that the sediments of LPS site was deposited during Marine Isotope Stage (MIS) 3 at the latest.

5 Discussion

5.1 Chronology of the LPS

The CAM, MaxAM and MinAM ages of sample 2019054 did not conform to the stratigraphic sequence, possibly indicating that the mineral particles of this sample have been exposed during the accumulation process. This phenomenon may be caused by the accumulation of cultural layers at the site. A long strip of gravel positioned at the top of the 5th cultural layer may have derived from ancient human activity or slope fluvial processes that exposed mineral particles in the cultural deposits (Fig. 2). The extraction of medium-grained sediment from a mixture with coarser grains always raises the possibility of medium grains being introduced by downward percolating water well after the initial deposition. Therefore, we believe that the buried age data of this layer cannot effectively indicate the true archaeological age and should not be considered. We combined the sedimentary characteristics and the ages of the 4th and 6th cultural layers; as a result, the 5th cultural layer was estimated to cover a period comprised between 46.59 ± 4.31 and 54.65 ± 7.39 ka approximately.

To summarize, the chronological sequence of the LPS could be roughly divided between a first (~54.65 - 46.58 ka) and a second (~27.93 to 27.09 ka) stage. This suggests that the Longdeng Mount area was occupied during this time (Fig. 6). The identified interval of time should have corresponded to a warm period, as suggested by the stalagmite oxygen isotope record (Hulu Cave, China) and the linking of the North Atlantic climate with the meridional transport of heat and moisture from the warmest part of the ocean (where the summer East Asian Monsoon originates) (Wang et al. 2008).

5.2 Palaeo-anthropocene activity at the LPS and climatic variation since MIS 3

The last glacial period, characterized by abrupt, millennial-scale climate changes, was an important period for the spread and evolution of early *Homo*
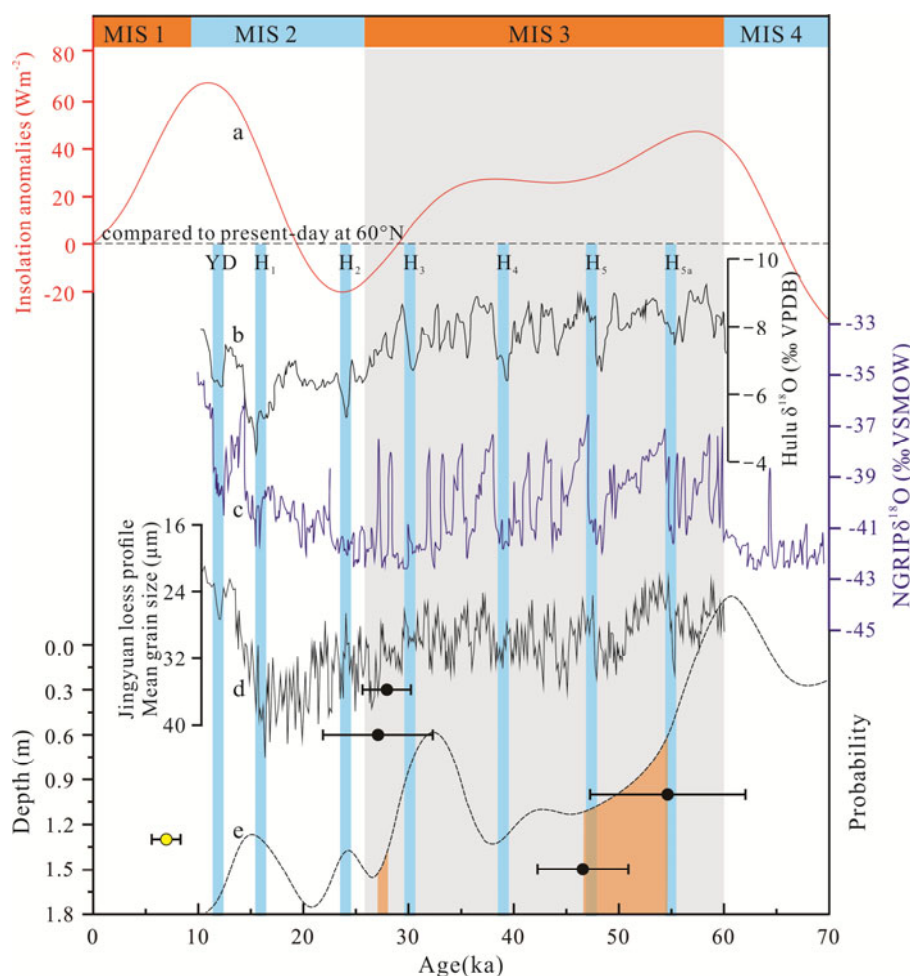

Fig. 6 Comprehensive comparisons between the climate records since MIS 3 and subsistence stages at the Longdengshan Palaeolithic site. (a) The red line represents the past insolation anomalies (compared to the present-day ones at 60°N) (Meerbeeck et al. 2009); (b) δ18O record of the Hulu Cave speleothem (Wang et al. 2008); (c) North GRIP δ18O curve (Andersen et al. 2004; Meerbeeck et al. 2009); (d) Changes in the strength of the EAWM over the past 60,000 years, which were reconstructed from the mean grain size in the Jingyuan loess profile (China); (e) The black dashed line represents the probability density curve of the chronology based on systematic optically stimulated luminescence age data of Fujian (China) (Jin et al. 2018).

sapiens in Asia, as well as for the flourishing of an upper Palaeolithic culture (Guan et al. 2011). This period was critical for the emergence and development of modern humans and their behaviours (Wang and Wang 2014). In China, the upper Palaeolithic culture was reflected by a binary distribution pattern of small stone tablets and large tools, which represented the main industry in the north and in the south, respectively (Fan et al. 2019; Wang and Wang 2014). Humans actively responded to the frequent fluctuations in the natural environment and climate during the Late Pleistocene, and left cultural heritages that reflected this behaviour. The LPS is a typical Palaeolithic site in southern China and was characterized, at the time of human settlements, by a large industry.

In order to comprehensively analyse the relationship between the sustainable time at the LPS and environmental changes, we compared the integrated insolation anomalies to those presently occurring at 60°N (Fig. 6). In the same figure are depicted the $\delta^{18}O$ record of Hulu Cave speleothem, the North Greenland Ice Core Project (GRIP) $\delta^{18}O$ curve, the mean grain size in the Jingyuan loess profile and the probability density curve of chronology for Fujian. The Heinrich events are marked by sky-blue rectangles on the diagram. Overall, the monsoonal proxy results indicate that a significant strengthening of the winter monsoon and a weakening of the summer monsoon were associated with strong cooling in the North Atlantic; these trends were particularly pronounced in records of the East Asian monsoon system (Meerbeeck et al. 2009; Sun et al. 2011; Wang et al. 2008).

Overall, the palaeoanthropocene activity period at the site coincided with one of strong solar irradiation (Fig. 6a), notably, the fluctuations in the reconstructed insolation anomaly curve are more obvious than those in the present insolation anomaly curve (based on observations at 60°N). The mean grain size along the Jingyuan loess profile may indicate changes in the strength of the East Asian winter monsoon (EAWM) over the past 60,000 years (Sun et al. 2011). The probability density curve of the chronology, based on systematic OSL age data may also indirectly indicate the strength of EAWM (Jin et al. 2018). As can be seen in Fig. 6b-e, the four OSL data were all distributed within MIS 3. This period represented a generally warm and wet phase (Meerbeeck et al. 2009; Wang et al. 2008), and can be roughly divided into two stages (Fig. 6), both included in the weakening phase of EAWM (Jin et al. 2018; Sun et al. 2011). A cultural break of ~15–20 ka may have occurred between the 3rd and 4th layer. At that time, the region should have experienced both a warm and a wet stage, as well as a strong EAWM stage; these are all clearly distinguishable in Fig. 6e. The warm and wet stage may explain the presence of the cobblestone strip in the archaeological layers, while the EAWM may represent the main natural factors for the cultural interruption at the site.

The Human presence occurred contemporaneous with Heinrich event H2 or H3 considering the error range of the ages (Fig. 6), when the global climate started to follow a new pattern and turned colder (i.e. start of the Last Glacial Maximum (LGM)). In that period, solar radiation was at its weakest since MIS 3 and, consequently, temperatures were much lower than today. Although the range of temperatures, the intensity of EAWM, the vegetation cover and the population type in Fujian during this period changed less than at global scale and in North China (Jin et al. 2018; Meerbeeck et al. 2009; Sun et al. 2011; Wang et al. 2008; Zhang et al. 2020), the variations induced by the LGM might have been the main factors causing the abandonment of the site.

Our new dating results indicate that the occupation of the Longdengshan hominids occurred in MIS 3 at the latest. Moreover, they provide a basis for the future studies on the interactions between the Longdengshan occupants and the local environment, and can support more accurate environmental reconstructions. Was the observed coupling between the hominid occupation and the warm wet climate during MIS 3 in South China an isolated case or a common phenomenon? To answer this question, we plan to establish reliable chronologies for additional Palaeolithic sites in South China. These would allow more in-depth discussions about the coupling relationship between humans and earth and the possible migration routes of human populations in the coastal areas of East Asia.

6   Conclusions

Our results indicate that the 38-63 mm quartz grains were generally partially bleached and presented large values of OD in the palaeo-reticulated laterites of west Fujian. Certain samples yield

unsatisfactory results, suggesting that the degree of bleaching of diluvial and alluvial deposits should be properly considered when dating such samples. We did not detect any enrichment/depletion of U, Th or radioactive disequilibrium; furthermore, the effect of chemical weathering on the dose rate estimation was negligible. Therefore, we used the CAM, MaxAM and MinAM model to calculate the ages of sample 2019055, 2019054 and 2019051-2019053, respectively. The model ages of sample 2019054 did not conform to those of the stratigraphic sequence, we believe that the buried age data of this layer cannot effectively indicate the true archaeological age and should not be considered. The calculation results show that the OSL ages of the samples ranged from 27.09 ± 5.22 ka to 54.65 ± 7.39 ka for the 38-63 µm quartz size fractions, corresponding roughly to MIS 3; additionally, they indicate that the occupation of the LPS can be divided into two stages (i.e. 54.7-46.6 ka, and 27.9-27.1 ka).

The LPS is close to the Wuyi Mountain (South China) and is of considerable significance for the studying the diffusion and culture of early *Homo sapiens* in southern China. Moreover, It represents the first discovered, scientifically excavated and the oldest well-dated Palaeolithic site in Fujian Province. The area in which the site is located was able to support human life due to the availability of sufficient water and food, and generally represented a suitable environment for living beings during MIS 3. Unfortunately, due to the absence of animal bones and other remains (which could have indicated the food exploitation choices of the time), we were not able to reconstruct the subsistence strategy of the Longdengshan occupants.

Acknowledgments

References

Adamiec G, Aitken M, (1998) Dose-rate conversion factors: update. Ancient TL 16(2): 37-50.

Aitken MJ, (1998) An introduction to optical dating: the dating of Quaternary sediments by the use of photon-stimulated luminescence. Oxford University Press.

Andersen KK, Azuma N, Barnola JM, et al. (2004) High-resolution record of Northern Hemisphere climate extending into the last interglacial period. Nature 431(7005): 147-51. https://doi.org/ 10.1038/nature02805

Arnold LJ, Bailey RM, Tucker GE (2007) Statistical treatment of fluvial dose distributions from southern Colorado arroyo deposits. Quat Geochronol 2 (1-4): 162-167. https://doi.org/10.1016/j.quageo.2006.05.003

Arnold LJ, Demuro M, Ruiz MN (2012) Empirical insights into multi-grain averaging effects from 'pseudo' single-grain OSL measurements. Radiat Meas 47(9): 652-658. https://doi.org/10.1016/j.radmeas.2012.02.005

Bøtter-Jensen L, Andersen C, Duller G, et al. (2003) Developments in radiation, stimulation and observation facilities in luminescence measurements. Radiat Meas 37(4): 535-541. https://doi.org/10.1016/S1350-4487(03)00020-9

Brennan BJ, Lyons RG, Phillips SW (1991) Attenuation of alpha particle track dose for spherical grains. International Journal of Radiation Applications and Instrumentation. Part D. Nuclear Tracks and Radiat Meas 18(1): 249-253. https://doi.org/10.1016/1359-0189(91)90119-3

Duller GAT (2003) Distinguishing quartz and feldspar in single grain luminescence measurements. Radiat Meas 37(2): 161-165. https://doi.org/10.1016/S1350-4487(02)00170-1

Durcan JA, King GE, Duller GAT (2015) DRAC: Dose Rate and Age Calculator for trapped charge dating. Quat Geochronol 28: 54-61. https://doi.org/10.1016/j.quageo.2015.03.012

Fan X, Zhou Z, Wang X, et al. (2019) Brief report on the excavation of Longdengshan Paleolithic site in west of Fujian Province, China. Fujian Wenbo (3): 2-7. (In Chinese)

Fu X, Li SH (2013) A modified multi-elevated-temperature post-IR IRSL protocol for dating Holocene sediments using K-feldspar. Quat Geochronol 17: 44-54. https://doi.org/10.1016/j.quageo.2013.02.004

Galbraith RF, Roberts RG (2012) Statistical aspects of equivalent dose and error calculation and display in OSL dating: An overview and some recommendations. Quat Geochronol 11: 1-27. https://doi.org/10.1016/j.quageo.2012.04.020

Galbraith RF, Roberts RG, Laslett GM, et al. (1999) Optical dating of single and multiple grains of quartz from Jinmium Rock shelter, northern Australia: part 1, experimental design and statistical models. Archaeometry 41(2): 339-364. https://doi.org/10.1111/j.1475-4754.1999.tb00987.x

Gao L, Long H, Shen J, et al. (2017) Optical dating of Holocene tidal deposits from the southwestern coast of the South Yellow Sea using different grain-size quartz fractions. J Asian Earth Sci 135: 155-165. https://doi.org/10.1016/j.jseaes.2016.12.036

Guan Y, Gao X, Li F, et al. (2011) Modern human behaviors during the late stage of the MIS3 and the broad spectrum revolution: Evidence from a Shuidonggou Late Paleolithic site. Chin Sci Bull 57(4): 379-386. https://doi.org/10.1007/s11434-011-4828-x

Guérin G, Mercier N, Nathan R, et al. (2012) On the use of the infinite matrix assumption and associated concepts: A critical review. Radiat Meas 47(9): 778-785. https://doi.org/10.1016/j.radmeas.2012.04.004

Guo Y, Li B, Zhang J, et al. (2017) New ages for the Upper Palaeolithic site of Xibaimaying in the Nihewan Basin, northern China: implications for small-tool and microblade

industries in north-east Asia during Marine Isotope Stages 2 and 3. J Quat Sci 32(4): 540-552. https://doi.org/10.1002/jqs.2949

Hu Y, Marwick B, Zhang J, et al. (2019) Late Middle Pleistocene Levallois stone-tool technology in southwest China. Nature 565(7737): 82-85. https://doi.org/10.1038/s41586-018-0710-1

Jacobs Z, Roberts RG, Lachlan TJ, et al. (2011) Development of the SAR TT-OSL procedure for dating Middle Pleistocene dune and shallow marine deposits along the southern Cape coast of South Africa. Quat Geochronol 6 (5): 491-513. https://doi.org/10.1016/j.quageo.2011.04.003

Jia L, Qiu Z (1960) The ages of strike stone in Gaungxi cave. Paleovertebrata et Paleoanthropologia 2(1): 64-68. (In Chinese)

Jin J, Li Z, Cheng Y, et al. (2018) Late Pleistocene aeolian activity in Haitan Island, Southeast China: Insights from optically stimulated luminescence dating of coastal dunes on marine terraces. J Mt Sci 15(8): 1777-1788. https://doi.org/10.1007/s11629-018-4890-9

Jin J, Li Z, Huang Y, et al. (2017) Chronology of a late Neolithic Age site near the southern coastal region of Fujian, China. Holocene 27(9): 1265-1272. https://doi.org/10.1177/0959683616687383

Lai Z, Mischke S, Madsen D (2013) Paleoenvironmental implications of new OSL dates on the formation of the "Shell Bar" in the Qaidam Basin, northeastern Qinghai-Tibetan Plateau. J Paleolimn 51(2): 197-210. https://doi.org/10.1007/s10933-013-9710-1

Lai Z, Zöller L, Fuchs M, et al. (2008) Alpha efficiency determination for OSL of quartz extracted from Chinese loess. Radiat Meas 43(2-6): 767-770. https://doi.org/10.1016/j.radmeas.2008.01.022

Li B, Li S-H (2011) Luminescence dating of K-feldspar from sediments: A protocol without anomalous fading correction. Quat Geochronol 6(5): 468-479. https://doi.org/10.1016/j.quageo.2011.05.001

Li S, Sun J, Zhao H (2002) Optical dating of dune sands in the northeastern deserts of China. Palaeogeogr Palaeoclimatol Palaeoecol 181(4): 419 - 429. https://doi.org/10.1016/s0031-0182(01)00443-6

Li Y (1982) On the relative age of the Paleolithic in Shouth China. Acta Anthropol Sin 1(2): 66-74. (In Chinese) https://doi.org/CNKI:SUN:RLXB.0.1982-02-008

Li Z, Wu X, Zhou L, et al. (2017) Late Pleistocene archaic human crania from Xuchang, China. Science 355(6328): 969-972. https://doi.org/10.1126/science.aal2482

Meerbeeck CJV, Renssen H, Roche DM (2009) How did Marine Isotope Stage 3 and Last Glacial Maximum climates differ? – Perspectives from equilibrium simulations. Clim Past 5: 33-51. https://doi.org/10.5194/cp-5-33-2009

Murray AS, Wintle AG (2000) Luminescence dating of quartz using an improved single-aliquot regenerative-dose protocol. Radiat Meas 32(1): 57-73. https://doi.org/10.1016/S1350-4487(99)00253-X

Nian X, Chen F, Li F, et al. (2015) Optical dating of a Paleolithic site near the eastern coastal region of Shandong, northern China. Quat Geochronol 30: 466-471. https://doi.org/10.1016/j.quageo.2015.02.009

Nian X, Zhang W, Wang Z, et al. (2018) Optical dating of Holocene sediments from the Yangtze River (Changjiang) Delta, China. Quat Int 467: 251-263. https://doi.org/10.1016/j.quaint.2018.01.011

Olsen JW, Miller-Antonio S (1992) The Palaeolithic in Southern China. Asian Perspect 31(2): 129-160.

Pei W (1955) Chinese paleolithic culture. Science Press, Beijing. (In Chinese)

Smedley RK, Duller GAT, Rufer D, et al. (2020) Empirical assessment of beta dose heterogeneity in sediments: Implications for luminescence dating. Quat Geochronol 56: 101052. https://doi.org/10.1016/j.quageo.2020.101052

Sun Y, Clemens SC, Morrill C, et al. (2011) Influence of Atlantic meridional overturning circulation on the East Asian winter monsoon. Nature Geosci 5(1): 46-49. https://doi.org/10.1038/ngeo1326

Wang Y (1997) Pleistocene environment and the development of Paleolithic culture in southern China. Peking University Press, Beijing. (In Chinese)

Wang Y, Cheng H, Edwards RL, et al. (2008) Millennial- and orbital-scale changes in the East Asian monsoon over the past 224,000 years. Nature 451(7182): 1090-3. https://doi.org/10.1038/nature06692

Wang Y, Wang S (2014) New Achievements and Perspectives on Paleolithic Archaeology During the MIS3 Along the Eastern Foot of Songshan Mountain, Henan Province. Acta Anthropol Sin 33(3): 304-314. (In Chinese) https://doi.org/CNKI:SUN:RLXB.0.2014-03-006

Zhang J, Li Y, Han Y, et al. (2019) Luminescence dating of weathered sediments from the Paleolithic site of Fengshuzui in northern Hunan province, China. Quat Geochronol 49: 211-217. https://doi.org/10.1016/j.quageo.2018.07.003

Zhang J, Nottebaum V, Tsukamoto S, et al. (2015) Late Pleistocene and Holocene loess sedimentation in central and western Qilian Shan (China) revealed by OSL dating. Quat Int 372: 120-129. https://doi.org/10.1016/j.quaint.2014.12.054

Zhang J, Yuan B, Zhou L (2008) Luminescence chronology of "Old Red Sand" in Jinjiang and its implications for optical dating of sediments in South China. Chinese Sci Bull 53(4): 591-601. https://doi.org/10.1007/s11434-008-0001-6

Zhang S (1983) On some problems of the upper Palaeolithic culture in Southern China. Acta Anthropol Sin 2(3): 218-230. https://doi.org/CNKI:SUN:RLXB.0.1983-03-001

Zhang X, Zhu L, Huang Y, et al. (2020). The reticulated mechanism and its climatic implication of aggradation red earth. Quat Sci 40(1): 214-228. https://doi.org/10.11928/j.issn.1001-7410.2020.01.20

Riedesel S, Autzen M (2020) Dose-rate conversion function. Function version 0.1.0. In: Kreutzer S, Burow C, Dietze M, et al., Luminescence: Comprehensive Luminescence Dating Data Analysis. R package version 0.9.10.